

## Electronic Supporting Information

### The gold(III)-CO bond: a missing piece in the gold carbonyl complexes landscape

Carlo Alberto Gaggioli,<sup>a</sup> Leonardo Belpassi,<sup>b\*</sup> Francesco Tarantelli,<sup>a,b</sup> Paola Belanzoni<sup>a,b\*</sup>

*a) Dipartimento di Chimica, Biologia e Biotecnologie, Università degli Studi di Perugia, Via Elce di Sotto 8, I-06123, Perugia, Italy*

*b) Istituto di Scienze e Tecnologie Molecolari del CNR (CNR-ISTM), c/o Dipartimento di Chimica, Biologia e Biotecnologie, Università degli Studi di Perugia, via Elce di Sotto 8, I-06123, Perugia, Italy*

1. Methodology.....	2
2. [(Idipp)AuCO] <sup>+</sup> vs. [(C <sup>^</sup> N <sup>^</sup> C)Au(III)(CO)] <sup>+</sup> bond properties .....	5
3. [(C <sup>^</sup> N <sup>^</sup> C)Au(III)(CO)] <sup>+</sup> vs. gold(I) carbonyls and homoleptic carbonyls: Δr <sub>CO</sub> vs. M <sup>→</sup> CO π back-donation CT <sup>π-back</sup> and CO π electron polarization CT <sup>π</sup> r <sub>CO/2</sub> .....	8
4. Electrostatic potential map of [(C <sup>^</sup> N <sup>^</sup> C)Au(III)] <sup>+</sup> and [(Idipp)Au(I)] <sup>+</sup> gold fragments.....	9
5. Model WGS reaction.....	10
6. Electrostatic potential map of [(C <sup>^</sup> N <sup>^</sup> C)Au(III)CO] <sup>+</sup> and [(Idipp)Au(I)CO] <sup>+</sup> complexes .....	12
7. References .....	13

## Methodology

### Computational Details

Geometry optimization and harmonic frequency calculations for the bond analysis (Charge-Displacement CD and Energy Decomposition Analysis EDA) have been performed at Density Functional Theory (DFT) level with the ADF package (version 2014.09)<sup>1,2,3</sup> using the Slater-type triple- $\zeta$  basis sets with two polarization functions (TZ2P) in the small frozen core approximation for all atoms and the GGA BLYP functional<sup>4,5</sup>. The zeroth-order regular approximation (ZORA) Hamiltonian has been employed to account for relativistic effects.<sup>6,7,8</sup> An assessment of such a level of theory has been given in the ESI of our previous work.<sup>9</sup> For reaction profile study, geometry optimization and harmonic frequency calculations have been carried out with Gaussian09 package<sup>10</sup> using the Def2-TZVP basis set and the GGA BP86 functional<sup>11,12</sup>, including Grimme 3 BJ damping dispersion effect (DFT-D3-BJ)<sup>13</sup>. Relativistic effects have been included using ECP for gold.

### Charge Displacement analysis (CD)

An efficient way to study thoroughly the rearrangement of the electron density taking place upon bond formation between two fragments A-B is *via* the Charge Displacement (CD) analysis. Within this framework a chemical bond A-B is described in terms of the difference between the electron density of the molecule AB and that of the two isolated non-interacting fragments A and B in the geometries they acquire in the overall molecule,  $\Delta\rho(x,y,z)$ . A partial progressive integration of  $\Delta\rho(x,y,z)$  along a suitable chosen bond axis  $z$  yields the so called Charge-Displacement Function (CDF). Mathematically, the CDF is defined as<sup>14</sup>:

$$\Delta q(z) = \int_{-\infty}^z dz' \int_{-\infty}^{\infty} dx \int_{-\infty}^{\infty} \Delta\rho(x,y,z') dy$$

At each point  $z$ , the CDF measures the exact amount of electron charge displaced from right to left (in the direction of decreasing  $z$ ) upon bond formation through a plane perpendicular to the  $z$  axis through the point  $z$ . Here  $z'$  denotes the reference axis, typically the axis joining the A and B fragments. Since the Au-CO bond in carbonyl complexes is under investigation in this work, suitable fragments are the ligand-metal moiety  $[\text{LAu}]^{0/+}$  and CO, and the  $z'$  reference axis joins the

Au and C centers. A positive (negative) value of  $\Delta q(z)$  indicates electrons moving towards the decreasing (increasing)  $z'$ . The CDF curve slope is a clear and immediate spatial picture of the charge flow: one can immediately visualize regions of charge accumulation (positive slope) or charge depletion (negative slope). If both the molecule and its constituting fragments have proper symmetry,  $\Delta\rho(x,y,z)$  can be decomposed into additive contributions from the distinct irreducible representations of the symmetry group with respect to the bond axis  $z'$ , and, in systems with a clear  $\sigma/\pi$  separation, into the very informative components of  $\sigma$  and  $\pi$  symmetry.<sup>15</sup> For this purpose we group the orbitals of the  $[(C^{\wedge}N^{\wedge}C)Au(III)-CO]^+$  complex and its constituting  $[(C^{\wedge}N^{\wedge}C)Au]^+$  and CO fragments, as well as of the  $[(Idipp)Au(I)-CO]^+$  complex and its  $[(Idipp)Au]^+$  and CO fragments, according to the irreducible representations of their common symmetry group which is  $C_{2v}$ , where the  $A_1$  representation corresponds to  $\sigma$  donation, while  $B_1$  and  $B_2$  correspond to out-of-plane ( $\perp$ ) and in-plane ( $\parallel$ )  $\pi$  back-donation, respectively. The  $A_2$  representation is not relevant within the Dewar-Chatt-Duncanson (DCD) model of the Au-CO bond (since no CO orbital is of  $A_2$  symmetry) and it accounts for only a minor rearrangement internal to the  $[(C^{\wedge}N^{\wedge}C)Au]^+$  and  $[(Idipp)Au]^+$  fragments.

To obtain well-defined measures of the net charge transfer and of its  $\sigma$  donation and  $\pi$  back-donation (in-plane  $\parallel$  and out-of-plane  $\perp$ ) contributions (hereafter denoted as  $CT^{net}$ ,  $CT^{\sigma-don}$ ,  $CT^{\pi-back \parallel}$  and  $CT^{\pi-back \perp}$ , respectively) CDF values at a plausible inter-fragment boundary can be taken. This choice is of course arbitrary, but a reasonable commonly used model is to take the CDF values at the so-called isodensity boundary, i.e. at the  $z'$  point where equal-valued isodensity surfaces of the fragments become tangent.<sup>15</sup> All of the CTs used in this work refer to the CTs taken at the isodensity boundary.

CDF also provides valuable additional information concerning CO polarization. Since the C-O bond is collinear with the Au-C  $z'$  axis of integration, the CDF in the C-O bond region represents the electron displacement within CO with respect to free CO in response to the Au-CO bond formation. A quantitative estimate of CO polarization, which can be also decomposed in  $\sigma$  and  $\pi$  components, is given by the amount of charge flowing across a plane perpendicular to the CO bond through its midpoint (i.e. the CDF value at  $z' = r_{CO/2}$ ). These values are referred as  $CT_{r_{CO/2}}$ ,  $CT^{\sigma}_{r_{CO/2}}$  and  $CT^{\pi}_{r_{CO/2}}$ , respectively.

## Energy Decomposition Analysis (EDA)

To study the Au(III)-CO and Au(I)-CO bonds, we also carried out the Energy Decomposition Analysis (EDA)<sup>16,17,18</sup> as implemented in the ADF package. The EDA approach allows to decompose the [(C<sup>^</sup>N<sup>^</sup>C)Au]<sup>+</sup>-CO and [(Idipp)Au]<sup>+</sup>-CO bond energy into contributions associated with the orbital, Pauli and electrostatic interactions. The interaction energy between two fragments A and B is decomposed into three terms:

$$\Delta E_{\text{int}} = \Delta E_{\text{elst}} + \Delta E_{\text{Pauli}} + \Delta E_{\text{oi}} = \Delta E^0 + \Delta E_{\text{oi}}$$

The first term  $\Delta E_{\text{elst}}$  is the electrostatic interaction of the nuclear charges and unmodified electronic charge density of one fragment with those of the other fragment, both fragments being at their final position. The second component  $\Delta E_{\text{Pauli}}$  is the so-called exchange repulsion or Pauli repulsion which is essentially due to the antisymmetry requirement on the total wavefunction, or equivalently the Pauli principle, leading to a depletion of electron density in the region of overlap between  $\psi^A$  and  $\psi^B$  and an increase in kinetic energy. It may be understood in a one-electron model as arising from the two-orbital four- or three-electron destabilizing interactions between occupied orbitals on the two fragments. The energy lowering due to mixing of virtual orbitals of the fragments into the occupied orbitals is called the orbital interaction energy,  $\Delta E_{\text{oi}}$  and it accounts for electron pair bonding, charge transfer and polarization. This term may be broken up into contributions from the orbital interactions within the various irreducible representations  $\Gamma$  of the overall symmetry group of the system,  $\Delta E_{\text{oi}} = \sum_{\Gamma} \Delta E(\Gamma)$ , which is very informative in systems with a clear  $\sigma/\pi$  separation. The sum of the electrostatic interaction  $\Delta E_{\text{elst}}$  and the Pauli repulsion  $\Delta E_{\text{Pauli}}$  terms,  $\Delta E^0$ , usually called the steric interaction energy, can be considered as a measure of the “ionic” contribution to the bond.

## $[(\text{Idipp})\text{AuCO}]^+$ vs. $[(\text{C}^{\wedge}\text{N}^{\wedge}\text{C})\text{Au}(\text{III})(\text{CO})]^+$ bond properties

For a close comparison between Au(III)-CO and Au(I)-CO bond, we also analyzed the  $[(\text{Idipp})\text{Au}(\text{CO})]^+$  complex, whose CD curves are reported in Figure S1.

### $[(\text{Idipp})\text{Au}(\text{I})\text{CO}]^+$

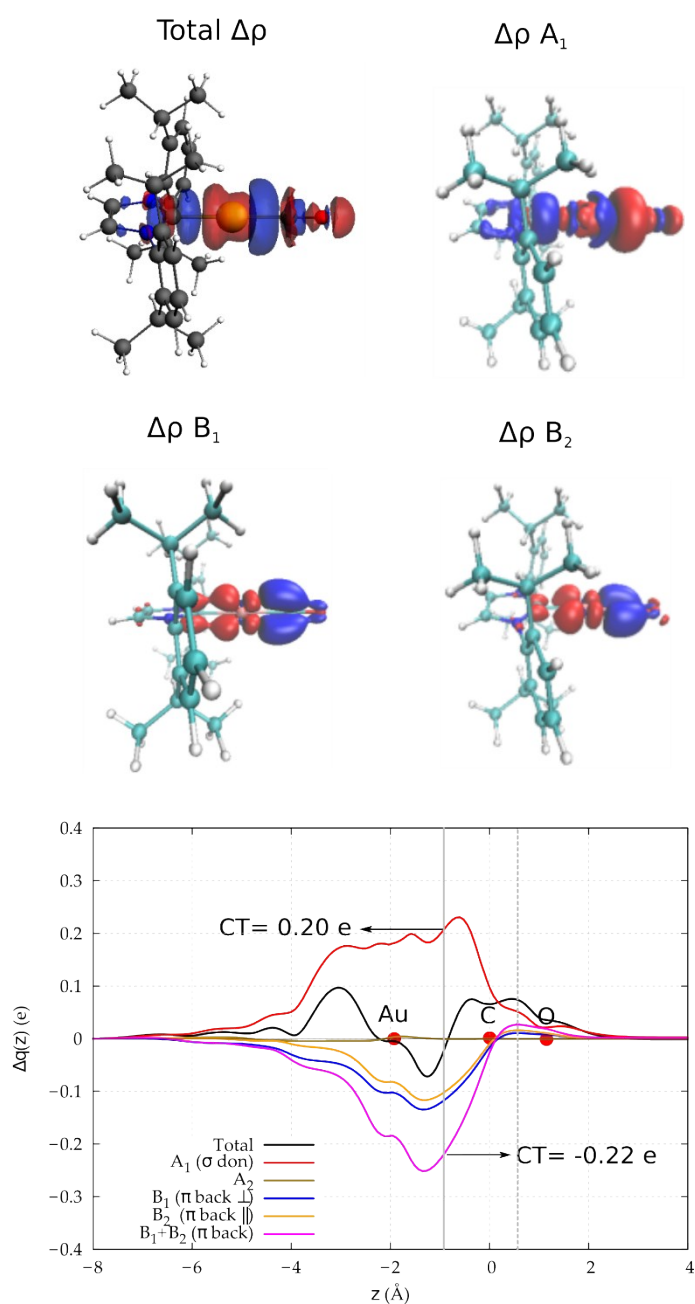


**Figure S1** Top: isodensity surfaces ( $\pm 0.001 \text{ e a.u.}^{-3}$ ) for the total  $\Delta\rho$  and its symmetry ( $C_{2v}$ )  $A_1$ ,  $B_1$  and  $B_2$  components for the Au-CO bond in  $[(\text{Idipp})\text{Au(I)-CO}]^+$  complex. Red surfaces indicate charge depletion regions, blue surfaces identify charge accumulation regions. Bottom: corresponding CDFs. Red dots represent the position of the atomic nuclei along the  $z$  axis. The solid vertical line marks the isodensity boundary between the  $[(\text{Idipp})\text{Au}]^+$  and the CO fragments (see Methodology). The dashed vertical line denotes the midpoint of the C-O bond ( $z = r_{\text{CO}/2}$ ).

This is very similar to Figure 1 in the main text, except that here the  $B_1$  (blue line) and  $B_2$  (yellow line) components are almost identical. The net charge transfer  $\text{CT}^{\text{net}}$  at the inter-fragment boundary is  $-0.02\text{e}$ , resulting from a  $\sigma$  donation component  $\text{CT}^{\sigma\text{-don}}$  of  $0.20\text{e}$  and a  $\pi$  back-donation component  $\text{CT}^{\pi\text{-back}}$  of  $-0.22\text{e}$  ( $-0.12\text{e}$  due to the out-of-plane and  $-0.10\text{e}$  due to the in-plane component). As for the polarization of the electron cloud in the carbonyl region, the  $\sigma$  CD curve remains positive in the CO area and both the  $\pi$ -backdonation CD components turn positive at the C site, reflecting the polarization of the CO bonding orbitals due to the electrostatic effect of the metal fragment. As a consequence, the CO bond is on the whole slightly polarized in the C  $\leftarrow$ O direction ( $\text{CT}_{r_{\text{CO}/2}} = 0.08\text{e}$ ), resulting from a  $\sigma$  polarization ( $\text{CT}_{r_{\text{CO}/2}}^{\sigma} = 0.05\text{e}$ ) and a  $\pi$  polarization ( $\text{CT}_{r_{\text{CO}/2}}^{\pi} = 0.02\text{e}$ ) in the same direction. On comparing the two complexes, the CD analysis reveals that the  $\sigma$  donation component of the Au-CO bond as well as the  $\pi$  back-donation is larger in  $[(\text{C}^{\wedge}\text{N}^{\wedge}\text{C})\text{Au(III)}(\text{CO})]^+$  ( $\text{CT}^{\sigma\text{-don}}$   $0.25\text{e}$  vs.  $0.20\text{e}$ ,  $\text{CT}^{\pi\text{-back}}$   $-0.28\text{e}$  vs.  $-0.22\text{e}$ , respectively), the  $\pi$  back-donation extent reducing the C  $\leftarrow$ O polarization of the CO bond. The polarization of the CO  $\sigma$  bonding orbitals is identical in the two complexes ( $\text{CT}_{r_{\text{CO}/2}}^{\sigma} = 0.05\text{e}$ ), but that of the  $\pi$  bonding orbitals is not ( $\text{CT}_{r_{\text{CO}/2}}^{\pi}$  is  $0.01\text{e}$  in  $[(\text{C}^{\wedge}\text{N}^{\wedge}\text{C})\text{Au(III)}(\text{CO})]^+$  vs.  $0.02\text{e}$  in  $[(\text{Idipp})\text{Au(I)-CO}]^+$ ). In particular, the  $\pi$ -back-donation CD component remains negative at the C site in  $[(\text{C}^{\wedge}\text{N}^{\wedge}\text{C})\text{Au(III)}(\text{CO})]^+$ , thus giving a more electropositive character to the C atom than that in the  $[(\text{Idipp})\text{Au}(\text{CO})]^+$  complex. This is clearly visible in the electrostatic potential maps for the two complexes reported in Figures S3 and S4. Finally, the out-of-plane  $\pi$  back-donation component in the Au-CO bond is roughly comparable in the two cases ( $-0.11\text{e}$  for  $[(\text{C}^{\wedge}\text{N}^{\wedge}\text{C})\text{Au(III)}(\text{CO})]^+$  vs.  $-0.12\text{e}$  for  $[(\text{Idipp})\text{Au(I)-CO}]^+$ ), whereas the in-plane  $\pi$  back-donation component is much larger in  $[(\text{C}^{\wedge}\text{N}^{\wedge}\text{C})\text{Au(III)}(\text{CO})]^+$  ( $-0.17\text{e}$  vs.  $-0.10\text{e}$ ).

## EDA analysis

All the CD analysis results are also supported by the Energy Decomposition analysis (EDA). The results of EDA analysis of the  $[(C^{\wedge}N^{\wedge}C)Au(III)-CO]^+$  and  $[(Idipp)Au(I)-CO]^+$  bond in the two complexes, performed considering cationic  $[(C^{\wedge}N^{\wedge}C)Au]^+$  and  $[(Idipp)Au]^+$ , respectively, and neutral CO as fragments, are shown in Table S1.

	$[(C^{\wedge}N^{\wedge}C)Au(III)-CO]^+$	$[(Idipp)Au(I)-CO]^+$
$\Delta E_{int}$	-48.4	-41.2
$\Delta E_{elst}$	-130.8	-117.5
$\Delta E_{Pauli}$	169.6	145.0
$\Delta E_{oi}$	-87.1	-68.7
$\Delta E_{A1}$	-54.4	-40.5
$\Delta E_{A2}$	-0.2	0.0
$\Delta E_{B1}$	-14.5	-14.6
$\Delta E_{B2}$	-18.1	-13.6

**Table S1** EDA analysis results for the  $[(C^{\wedge}N^{\wedge}C)Au(III)-CO]^+$  and  $[(Idipp)Au(I)-CO]^+$  bonds. All energies are in kcal/mol.

The orbital energy for the  $A_1$  component ( $\Delta E_{A1}$ ) is larger for the Au(III)-CO than that for Au(I)-CO bond (-54.4 vs. -40.5 kcal/mol) reflecting the larger  $\sigma$  donation component in the Au(III)-CO bond. In particular, the orbital energy for the  $B_2$  component ( $\Delta E_{B2}$ ) is larger for the Au(III)-CO bond (-18.1 vs. -13.6 kcal/mol) in agreement with the larger component of the Au(III)-CO in-plane  $\pi$  back-donation, while the orbital energy for the  $B_1$  component ( $\Delta E_{B1}$ ) is almost identical (-14.5 vs. -14.6 kcal/mol) in agreement with the comparable out-of-plane  $\pi$  back-donation component in Au(III)-CO and Au(I)-CO. The different  $\pi$  polarization of CO, which translates into a different electrophilic character of CO carbon atom, and the asymmetric/symmetric  $\pi$  back-donation component in the Au(III)-CO/Au(I)-CO bond seems to suggest pronounced differences in the catalytic activity.

**$[(C^{\wedge}N^{\wedge}C)Au(III)(CO)]^+$  vs. gold(I) carbonyls and homoleptic carbonyls:  $\Delta r_{CO}$  vs.  $M \rightarrow CO \pi$  back-donation  $CT^{\pi-back}$  and  $CO \pi$  electron polarization  $CT^{\pi} r_{CO/2}$**

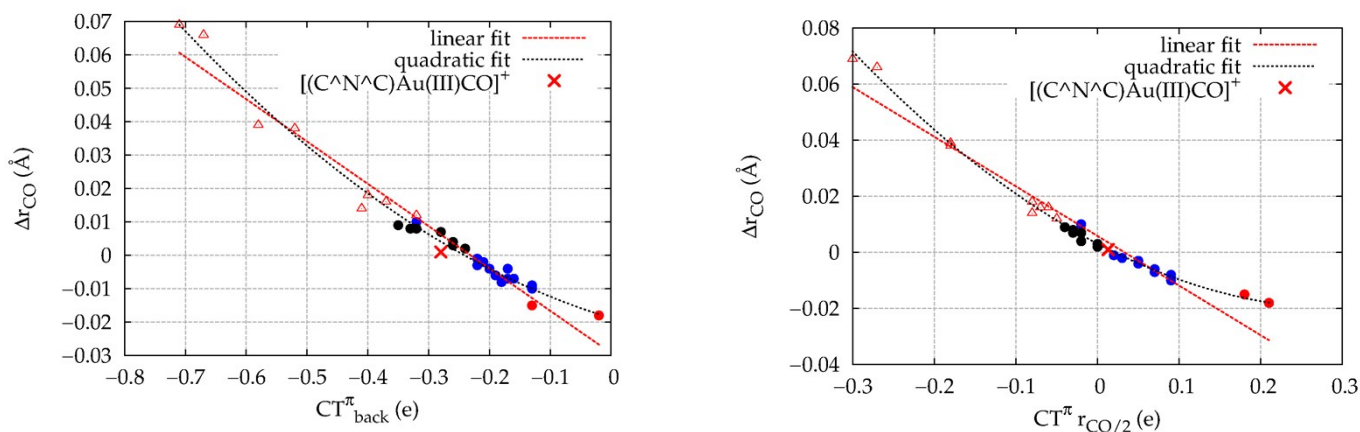


**Figure S2.** Correlation plot between CO bond-length change upon coordination to Au,  $\Delta r_{CO}$ , and left)  $M \rightarrow CO \pi$  back-donation  $CT^{\pi-back}$ , right)  $CO \pi$  electron polarization  $CT^{\pi} r_{CO/2}$ , for the whole series of complexes studied in ref. 9. Red cross refers to  $[(C^{\wedge}N^{\wedge}C)Au(III)CO]^+$  complex, blue (black) dots to the cationic (neutral) gold(I) carbonyls, and red colored points to the homoleptic carbonyls (dots for positively charged complexes, empty triangles for neutral or negatively charged complexes).

## Electrostatic potential maps

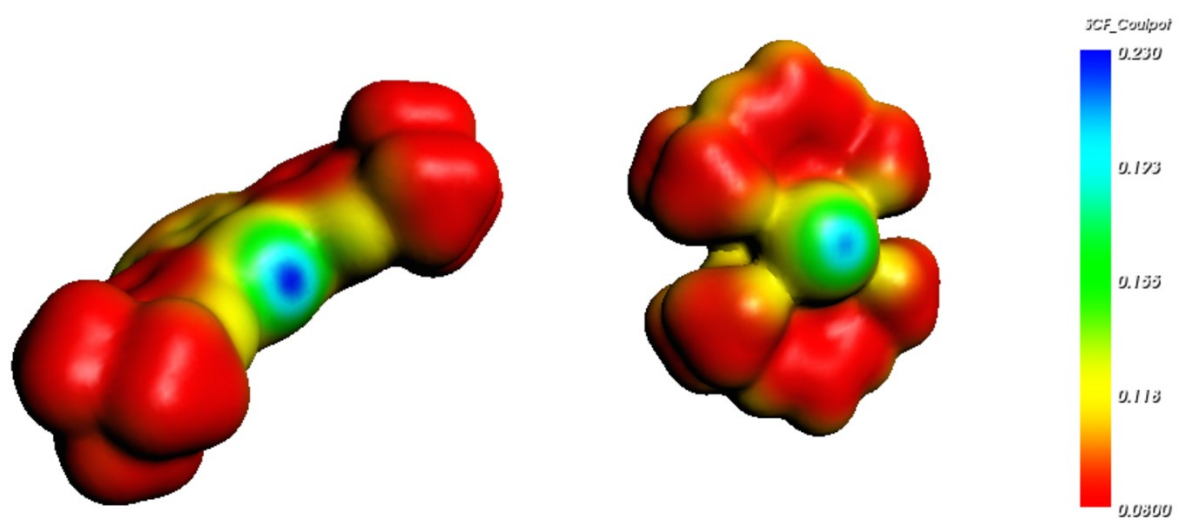


**Figure S3** Electrostatic potential maps (isodensity 0.001 e/au) of left)  $[(C^{\wedge}N^{\wedge}C)Au(III)]^{+}$  and right)  $[(Idipp)Au(I)]^{+}$  gold fragments.

## Model WGS reaction

To explore the water-gas shift (WGS) reaction we performed DFT calculations using a simplified model of the Au(III) complex, with the t-Bu groups on the ligand replaced by hydrogen atoms, and of the Au(I) complex, with the Ar groups on the ligand replaced by methyl groups. We initially tried to carry out the model complexes  $[(C^{\wedge}N^{\wedge}C)Au(III)-CO]^+$  and  $[(Idipp)Au(I)-CO]^+$  reaction using only  $H_2O$  or  $OH^-$  as nucleophiles, but we have not been able to calculate a stable product and a stable reactant, respectively. With  $H_2O$  the product is a protonated acid, while  $OH^-$  immediately reacts with Au, producing a gold hydroxyl complex and displacing CO. So we decided to analyze the reaction using  $H_2O$  assisted in its nucleophilic attack to CO by the OTf (trifluoromethanesulfonate, triflate) anion. The experimental anion in ref. 19 is  $[B(C_6F_5)_3(CF_3COO)]^-$ , which is a weak coordinating one. We therefore chose OTf since is a smaller anion and it is suitable for simulating the weak coordinating power of the experimental counterion. We carried out scans of the potential energy surface as oxygen atom of  $H_2O$  approaches the carbon atom of CO in the two model complexes and in Figure S4 the reaction profiles, starting from the reactant complexes (RC) to the product complexes (PC), are shown. For the Au(III)-CO complex the reaction is barrierless and exothermic by 9.1 kcal/mol, while for the Au(I)-CO complex the reaction is endothermic by 11.7 kcal/mol. A Transition State (TS) has been found very much product-like (TS is 12.6 kcal/mol above the RC). We should mention here that we have been able to locate the TS only by performing a two dimensional potential energy surface scan with a step of 0.05 Å, attesting the difficulty of finding this TS. The two scanned coordinates were the O ( $H_2O$ )-C (CO) distance and the H ( $H_2O$ )-O (OTf) distance. We find that the carbon atom in the Au(III)-CO complex is sufficiently electropositive to easily undergo the  $H_2O$  nucleophilic attack, but the carbon atom in Au(I)-CO is not. Interestingly, a sample geometrical structure taken along the scan (at a  $H_2O$ -CO distance of 1.81 Å) reveals that the  $H_2O$  attack occurs perpendicularly to the molecular plane in the Au(III)-CO complex (with a N-Au-C(CO)-O( $H_2O$ ) dihedral angle of 9.6°) and in a less well-defined direction with respect to the molecular plane in the Au(I)-CO complex (C-Au-C(CO)-O( $H_2O$ ) dihedral angle of 63.0°), as shown in Figure S5, thus probing the asymmetric  $\pi$  back-donation component in the Au(III)-CO which favors the nucleophile perpendicular attack.

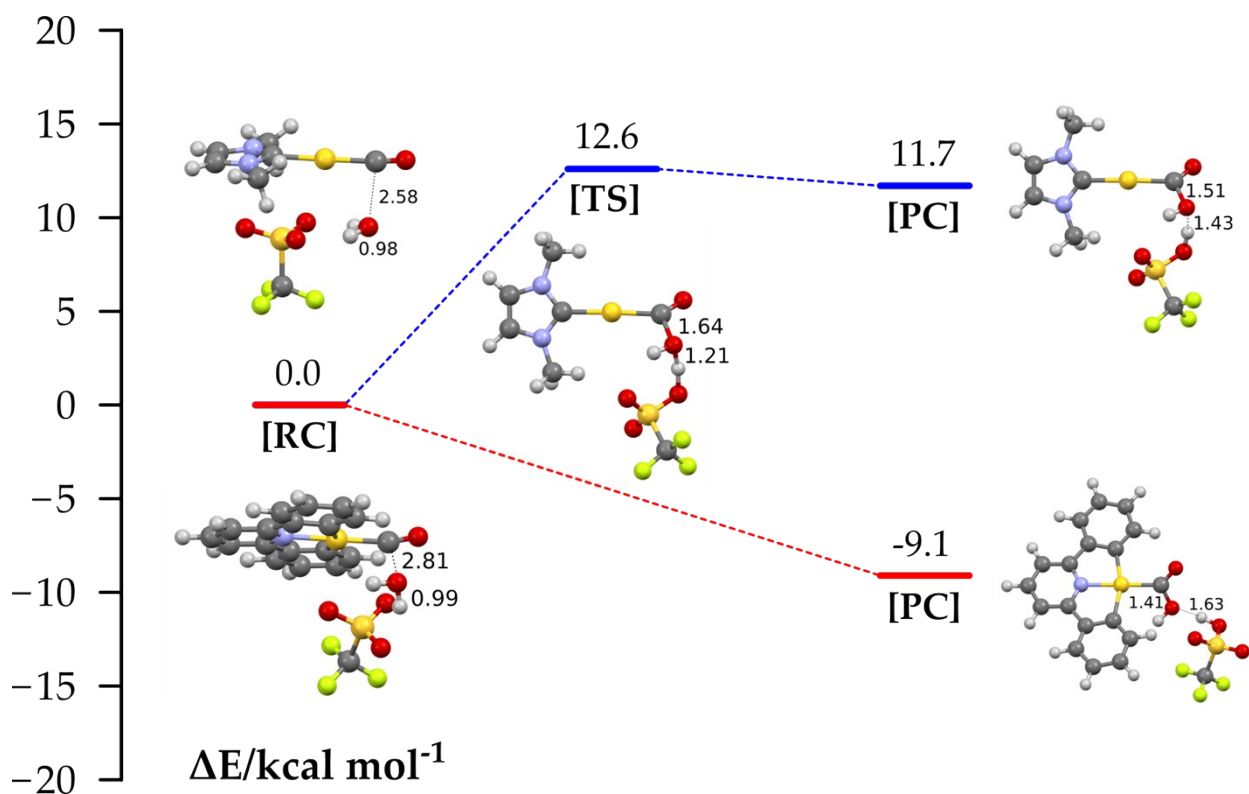


**Figure S4** Reaction profile for the OTf-assisted  $\text{H}_2\text{O}$  nucleophilic attack on CO carbon atom in two model complexes for Au(III) and Au(I). Energies are given in kcal/mol with respect to the reactant complexes RC taken as zero point energy.

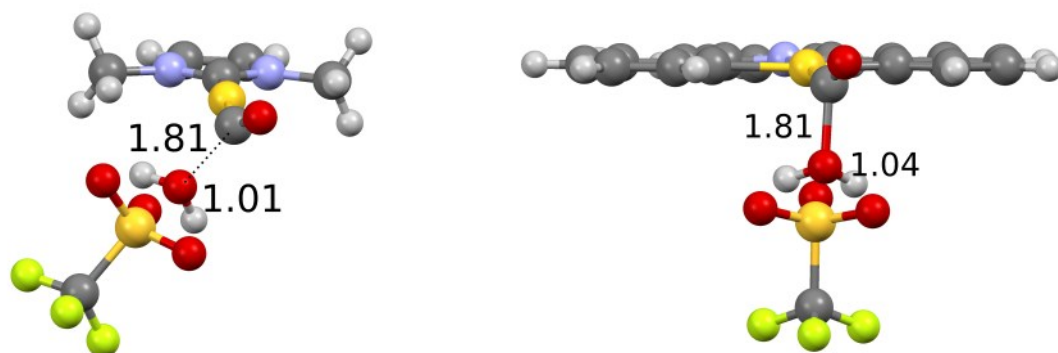


**Figure S5** Reacting structures taken along the potential energy scan at a  $\text{H}_2\text{O}$ -CO distance of 1.81 Å for the left) Au(I) and right) Au(III) model complex reactions.

## Electrostatic potential maps

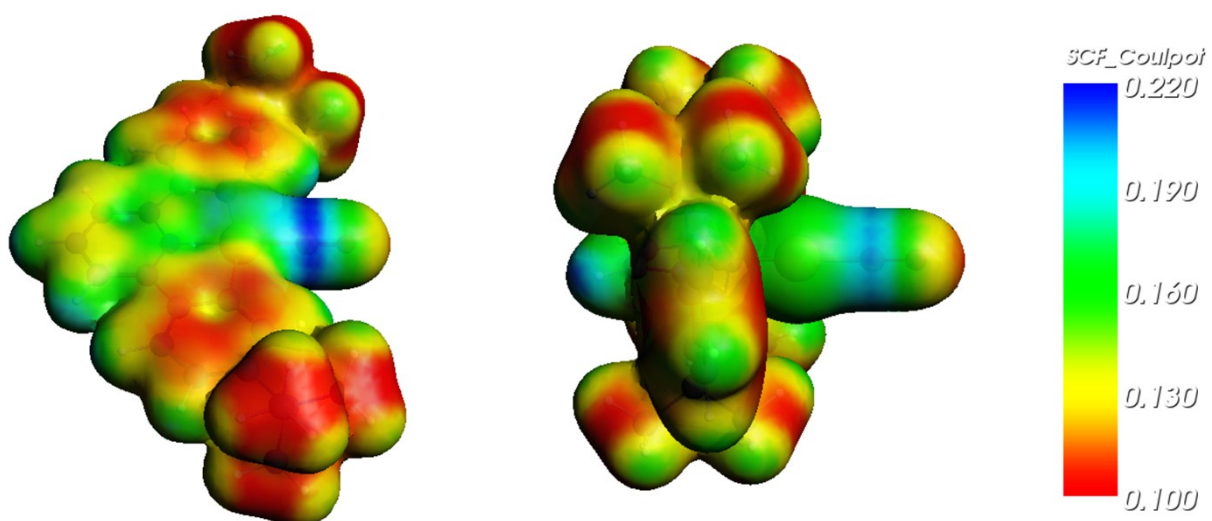


**Figure S6** Electrostatic potential maps (isodensity 0.007 e/au) of left)  $[(C^{\wedge}N^{\wedge}C)Au(III)CO]^+$  and right)  $[(Idipp)Au(I)CO]^+$  complexes.

## References

- <sup>1</sup> SCM, Theoretical Chemistry, *ADF User's Guide. Release 2014.09*, Vrije Universiteit, Amsterdam, The Netherlands, 2014. <http://www.scm.com>
- <sup>2</sup> C. Fonseca Guerra, J. G. Snijders, G. te Velde and E. J. Baerends, *Theor. Chem. Acc.*, 1998, **99**, 391-403.
- <sup>3</sup> G. te Velde, F. M. Bickelhaupt, E. J. Baerends, C. Fonseca Guerra, S. J. A. van Gisbergen, J. G. Snijders and T. Ziegler, *J. Comput. Chem.*, 2001, **22**, 931-967.
- <sup>4</sup> A. D. Becke, *Phys. Rev. A: At., Mol., Opt. Phys.*, 1988, **38**, 3098-3100.
- <sup>5</sup> C. Lee, W. Yang and R. G. Parr, *Phys. Rev. B: Condens. Matter Mater. Phys.*, 1988, **37**, 785-789.
- <sup>6</sup> E. van Lenthe, E. J. Baerends and J. G. Snijders, *J. Chem. Phys.*, 1993, **99**, 4597-4610.
- <sup>7</sup> E. van Lenthe, E. J. Baerends and J. G. Snijders, *J. Chem. Phys.*, 1994, **101**, 9783-9792.
- <sup>8</sup> E. van Lenthe, A. Ehlers and E. J. Baerends, *J. Chem. Phys.*, 1999, **110**, 8943-8953.
- <sup>9</sup> G. Bistoni, S. Rampino, N. Scafuri, G. Ciancaleoni, D. Zuccaccia, L. Belpassi and F. Tarantelli, *Chem. Sci.*, 2016, **7**, 1174-1184.
- <sup>10</sup> M.J. Frisch, G.W. Trucks, H.B. Schlegel, G.E. Scuseria, M.A. Robb, J.R. Cheeseman, G. Scalmani, V. Barone, B. Mennucci, G.A. Petersson, H. Nakatsuji, M. Caricato, X. Li, H.P. Hratchian, A.F. Izmaylov, J. Bloino, G. Zheng, J.L. Sonnenberg, M. Hada, M. Ehara, K. Toyota, R. Fukuda, J. Hasegawa, M. Ishida, T. Nakajima, Y. Honda, O. Kitao, H. Nakai, T. Vreven, J.A. Jr. Montgomery, J.E. Peralta, F. Ogliaro, M. Bearpark, J.J. Heyd, E. Brothers, K.N. Kudin, V.N. Staroverov, R. Kobayashi, J. Normand, K. Raghavachari, A. Rendell, J.C. Burant, S.S. Iyengar, J. Tomasi, M. Cossi, N. Rega, J.M. Millam, M. Klene, J.E. Knox, J.B. Cross, V. Bakken, C. Adamo, J. Jaramillo, R. Gomperts, R.E. Stratmann, O. Yazyev, J. Austin, R. Cammi, C. Pomelli, J.W. Ochterski, R.L. Martin, K. Morokuma, V.G. Zakrzewski, G.A. Voth, P. Salvador, J.J. Dannenberg, S. Dapprich, A.D. Daniels, O. Farkas, J.B. Foresman, J.V. Ortiz, J. Cioslowski and D.J. Fox, *Gaussian 09, revision A.02*, Gaussian Inc., Wallingford, CT, 2009.
- <sup>11</sup> A.D. Becke, *Phys. Rev. A: At., Mol., Opt. Phys.*, 1988, **38**, 3098.
- <sup>12</sup> J.P. Perdew, *Phys. Rev. B: Condens. Matter Mater. Phys.*, 1986, **33**, 8822.
- <sup>13</sup> S. Grimme, S. Ehrlich and L. Goerigk, *J. Comput. Chem.*, 2011, **32**, 1456.
- <sup>14</sup> L. Belpassi, I. Infante, F. Tarantelli and L. Visscher, *J. Am. Chem. Soc.*, 2008, **130**, 1048-1060.
- <sup>15</sup> N. Salvi, L. Belpassi and F. Tarantelli, *Chem.-Eur. J.*, 2010, **16**, 7231-7240.
- <sup>16</sup> K. Morokuma, *J. Chem. Phys.*, 1971, **55**, 1236-1244.
- <sup>17</sup> T. Ziegler and A. Rauk, *Theor. Chim. Acta*, 1977, **46**, 1-10.
- <sup>18</sup> M. von Hopffgarten and G. Frenking, *WIREs Comput. Mol. Sci.*, 2012, **2**, 43-62.
- <sup>19</sup> D.-A. Roşca, J. Fernandez-Cestau, J. Morris, J. A. Wright and M. Bochmann, *Sci. Adv.*, 2015, **1**, e1500761.